Available online at www.sciencedirect.com
SCIENCE DIRECT®
International Journal of Solids and Structures 42 (2005) 647–661
INTERNATIONAL JOURNAL OF SOLIDS and STRUCTURES
www.elsevier.com/locate/ijsolstr

Predictions of strength in MEMS components with defects—a novel experimental–theoretical approach

N. Pugno [1], B. Peng, H.D. Espinosa *

Department of Mechanical Engineering, Northwestern University, 2145 Sheridan Rd., Evanston, IL 60208-3111, USA

Received 25 May 2004
Available online 11 August 2004

Abstract

This paper presents a novel experimental–theoretical method to investigate the strength of structures having complex geometries, which are commonly used in microelectromechanical systems (MEMS). It involves the stretching to failure of freestanding thin-film membranes, in a fixed–fixed configuration, containing micro-fabricated sharp cracks, blunt notches and re-entrant corners. The defects, made by nanoindentation and focused ion beam milling, are characterized by scanning electron microscopy (SEM). MEMS structures made of ultra-nano-crystalline-diamond (UNCD), a material developed at Argonne National Laboratory, were investigated using this methodology. A theory to predict the strength of microstructures with defects is proposed and compared with experimental results. It is shown that fracture mechanics general concepts can be applied with confidence in the design of MEMS. An experimental methodology and formulas to predict strength of MEMS structures possessing defects of various geometries are provided.

Keywords: Thin films; Fracture; Strength; MEMS; Brittle materials

1. Introduction

Significant research has been conducted on the design, modeling, and manufacturing of microelectromechanical systems (MEMS). However, long-term durability of various MEMS devices requires a fundamental understanding of the failure characteristics of micro-fabricated structures such as fracture strength and fracture toughness.

* Corresponding author. Tel.: +1 847 467 5989; fax: +1 847 491 3915.
E-mail address: espinosa@northwestern.edu (H.D. Espinosa).
[1] On leave from Department of Structural Engineering, Politecnico di Torino, Corso Duca degli Abruzzi 24, 10129 Torino, Italy.

0020-7683/$ - see front matter
doi:10.1016/j.ijsolstr.2004.06.026

Several micro-scale testing techniques have been employed to investigate fracture toughness or fracture strength of thin films. Ballarini et al. (1997) and Kahn et al. (2000) used polysilicon fracture specimens integrated with on-chip fabricated electrostatic comb-drive actuators. The devices were tested using DC electrostatic actuation and the displacements were measured using an optical microscope. The measured fracture toughness, K_{IC}, of polysilicon showed a median value of 1.1 MPa m$^{1/2}$, which was found to be independent of polysilicon microstructure. The advantage of this technique is that the entire fracture experiment is performed at the chip level, thus, eliminating difficulties associated with attaching the specimens to external loading sources.

Sharpe et al. (1999, 2001) and Jackson et al. (2002), have performed microsample tension tests to study the fracture strength of SiC and polysilicon. The specimens were manufactured by surface micromachining with one end attached to the silicon wafer. The gage section and the grip end of the specimen were released by etching away the underlying sacrificial layer. A probe was attached to the grip end of the specimen, which was pulled by a piezoelectric translation stage. Force was measured with a 100 g load cell and overall system displacement was measured with a capacitance probe. The strain was measured directly on the specimen via laser interferometry. Young's modulus was extracted from the force–displacement curve by comparing the records of specimens of different lengths to eliminate the need to know the system stiffness. Using this technique, the strength of several thin film materials were determined. For polysilicon, the measured strength was found to be highly dependent on the film deposition parameters. A strength of 1.56 ± 0.25 GPa was measured for the Cronos fabrication, 2.85 ± 0.40 GPa for the Sandia process, and 2.04 ± 0.30 GPa for the SMI process. When measuring the fracture toughness of polysilicon the specimens were micro-fabricated with notches of 1.0 μm in radius. They reported a critical stress intensity factor, K_{IC}, of 1.4 MPa m$^{1/2}$ associated with the finite radius of the notches. Thus, the measurement does not represent the true fracture toughness of the material as we will show in the theoretical section of this paper.

Chasiotis and Knauss (2000, 2001), performed tensile tests, using a sample geometry and loading stage similar to the one used by Sharpe et al. (1999, 2001, 2002), to investigate the mechanical strength and fracture toughness of polysilicon films. A "dog-bone-shaped" tensile micro-specimen was employed, with test section dimensions of length = 400 μm, width = 50 μm, and thickness = 2 μm, attached at one end to a silicon substrate. Displacements were imposed to the specimen via an inchworm actuator that was powered by a personal computer and a dedicated controller. The controller provided a measurement of the system displacement with an accuracy of 4 nm for every single step of the actuator. The induced load was measured by a miniature tension/compression load cell with an accuracy of 10^{-4} N and maximum capacity of 0.5 N. In this case, the local deformation field was monitored directly on the specimen surface by means of AFM digital image correlation. These researchers measured a fracture strength of 1.3 ± 0.1 GPa for the Cronos process, which is slightly smaller than the one measured by Sharpe et al. (1999, 2001, 2002). The stress intensity, K_I, was obtained by this method using perforated specimens. As a result, fracture toughness was not measured but rather the materials strength at stress concentrations (Chasiotis and Knauss, 2002).

Espinosa et al. (2003a,b,c, 2004) employed a membrane deflection experiment to investigate the mechanical properties of thin film materials. This technique offers certain advantages such as the loading procedure is straightforward and accomplished in a highly sensitive manner while preserving the independent measurement of stress and strain (Espinosa et al., 2003a). The simplicity of sample micro-fabrication and ease of handling make this technique suitable for routine on-chip screening of material properties. As an example, the strength and the material properties of UNCD thin films were investigated. This material was developed at Argonne National Laboratory and possesses unique properties particularly suitable to the development of novel MEMS/NEMS devices (Gruen, 1999; Espinosa et al., 2003b). The measured fracture strength of UNCD is in the range of 4.2 ± 0.9 GPa and follows the Weibull distribution (Espinosa et al., 2003c). The high stiffness (960 GPa Young's modulus) and brittleness of UNCD make the measurement of its facture strength and toughness particularly challenging. However, the MDE experimental approach is capable of providing sufficient force and elongation to ensure crack propagation.

The problem in evaluating the strength of MEMS structures is further complicated by the fact that they are often designed with blunt notches and re-entrant corners. Furthermore, sharp cracks can result as a consequence of the micro-fabrication process or as a consequence of pre-existing defects. Accordingly, the evaluation of the strength for micro-structures containing sharp cracks, blunt notches and re-entrant corners, seems to be a fundamental step towards an optimal MEMS design.

On the other hand, from a different viewpoint, the understanding of such phenomenon would allow for corrections on the experimentally obtained stress-intensity factors, when a perfectly sharp crack instead of a real micro-fabricated blunt notch is assumed. Usually, we can assume an ideal crack (with an atomic tip radius) if it is obtained by propagating pre-exiting defects. Nevertheless, a blunt notch has to be considered if a crack-like defect is obtained in the specimen by a cut (e.g., ion beam cutting).

The evaluation of the influence of the radius of the blunt notch, in the fracture behavior at the micro-scale is not trivial as emphasized by Drory et al. (1995). They propose a blunt correction due to the notch radius by equating the asymptotic stress fields of a blunt notch and of a sharp crack. Unfortunately, as mentioned by the same authors, an uncertainty remains in the selection of the radial distance use to equate the two stress fields. Therefore, only a conservative estimate is suggested.

Recently, Espinosa and Peng (2004) presented a technique to investigate the fracture toughness of MEMS materials and thin films. These authors illustrated the technique by identifying the fracture toughness of UNCD. They found that when the fracture initiates from sharp cracks, produced by nanoindentation, the fracture toughness was found to be 4.5 $\mathrm{MPa\,m^{1/2}}$. When the fracture initiates from blunt notches with radii about 100 nm, machined by focused ion beam (FIB), the mean value of the apparent fracture toughness was found to be 6.9 $\mathrm{MPa\,m^{1/2}}$. Using, as a first approximation, the blunt notch correction proposed by Drory et al. (1995), they fit their experiment results and showed that a better estimate is found when the mean value of $\rho/2x = 1/2$ is employed (Espinosa and Peng, 2004).

Since it is clear that a better understanding of the effect of blunting is needed, in this paper we present an analysis aimed to evaluate in a rigorous way this effect, as well as that of re-entrant corners. In the later, formulas developed by Carpinteri and Pugno (2000, 2003) are employed. We begin the paper by describing the experimental approach. A description of tested MEMS specimens, made of UNCD, is provided. A section follows in which the strength of micro-tensile specimens, with and without sharp cracks, notches and re-entrant corners are reported. Interpretation of these experiments using fracture mechanisms theory is then discussed. We next show by employing fracture mechanics ideas that a well-defined criterion for predicting the strength of MEMS structures, having a variety of defects, exists. We conclude with some general remarks and comments on the applicability of the experimental–theoretical approach.

2. Experimental procedure

In order to investigate the strength of freestanding thin films, with and without defects, the membrane deflection experiment is used (Espinosa et al., 2003a). The technique involves the stretching of freestanding specimens in a fixed–fixed configuration with submicron thickness. The specimen geometry utilized in this study resembles the typical dog-bone tensile specimen but with an area of additional width in the specimen center designed to prevent failure at the point of application of a line load (see Fig. 1a). The suspended membranes are fixed to the wafer at both ends such that they span a bottom view window (Fig. 1b). In the areas where the membrane is attached to the wafer and in the central area the width is varied in such a fashion to minimize boundary-bending effects. These effects are also minimized through large specimen gauge lengths. Thus, a line load applied in the center of the span results in direct stretching under large displacements of the membrane, in the two areas of constant width, in the same manner as in a direct tension test. In this study, UNCD membranes with nominal dimensions of length $L_{\mathrm{M}} = 329$ μm, width $W = 20$ μm, and thickness, $t = 0.8$ μm, were tested (see Fig. 1b). The films are grown directly onto a Si substrate using a

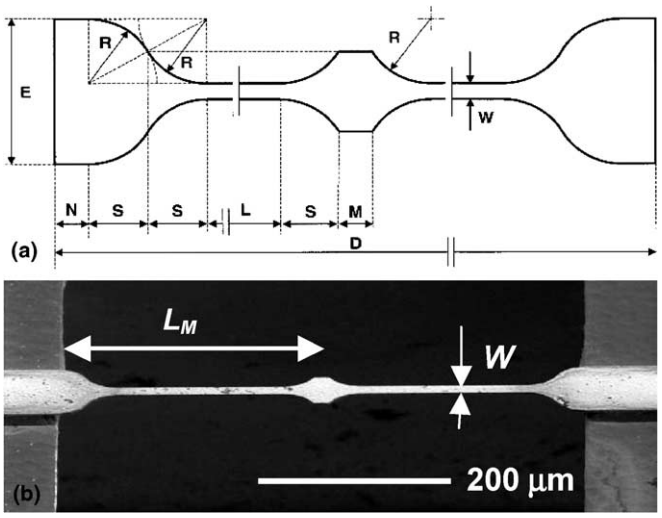

Fig. 1. (a) Schematic of membrane geometry indicating the various parameters used to define the tested specimen dimensions; where $E = 100$ μm, $R = 40$ μm, $W = 20$ μm, $N = 20$ μm, $L = 200$ μm, $S = 34.64$ μm, $M = 10$ μm, $D = 657.84$ μm. (b) Scanning electron microscopy (SEM) image of UNCD membrane showing characteristic dimensions. L_M is half the membrane span and W is the membrane width.

microwave plasma chemical vapor deposition technique involving a novel CH4/Ar chemistry (Gruen, 1999). The specimen structures were micro-fabricated using standard techniques as described by Espinosa et al. (2003b,c, 2004).

The testing procedure involves applying a line-load, with a nanoindenter, at the center of the spanning membrane (see Fig. 2a). Simultaneously, an interferometer focused on the bottom side of the membrane records the deflection. The result is direct tension of the gauged regions, in the absence of strain gradients, with load and deflection being measured independently.

The data directly obtained from the experiment is processed to arrive at a stress–strain signature for the membrane. The load in the plane of the membrane is found as a component of the vertical nanoindenter load by the following equations:

$$\tan\theta = \frac{\Delta}{L_{\mathrm{M}}} \quad \text{and} \quad P_{\mathrm{M}} = \frac{P_V}{2\sin\theta}, \tag{1}$$

where (from Fig. 2a) θ is the angle of deflection, Δ is the displacement, L_{M} is the membrane half-length, P_{M} is the load in the plane of the membrane, and P_V is the load measured by the nanoindenter. Once P_{M} is obtained at each time t, the Cauchy stress, $\sigma(t)$, can be computed from:

$$\sigma(t) = \frac{P_{\mathrm{M}}}{A}, \tag{2}$$

where A is the cross-sectional area of the membrane in the gauge region.

The interferometer yields vertical displacement information in the form of monochromatic images taken at periodic intervals (see Fig. 2b). The relationship for the distance between fringes, δ, is related through the wavelength λ of the monochromatic light used (see Fig. 2c). Assuming that the membrane is deforming uniformly along its gauge length, the relative deflection between two points can be calculated, independently of the nanoindenter measurements, by counting the total number of fringes and multiplying by $\lambda/2$. Normally part of the membrane is out of the focal plane and thus all fringes cannot be counted. By finding the

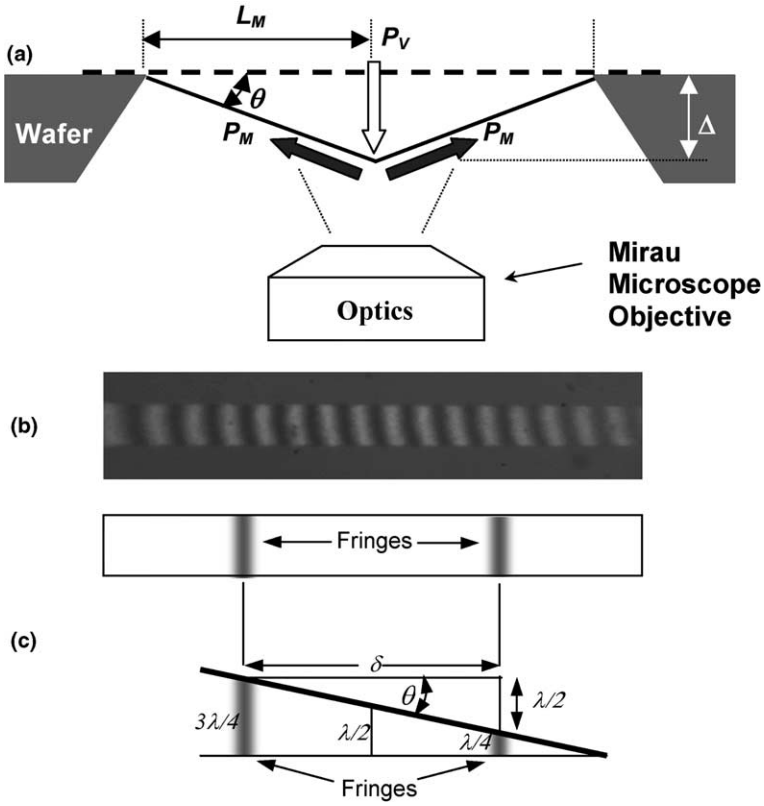

Fig. 2. (a) Schematic of the experimental setup. Parameters are defined in the text. (b) Monochromatic images of the bottom side of the membranes showing a membrane under load which has developed fringes. (c) A schematic representation showing the relationship between distance between fringes (δ) and vertical displacement. The distance between fringes is taken at the central points of the dark bands.

average distance between the number of fringes that are in the focal plane of the interferometer, an overall strain, $\varepsilon(t)$, for the membrane can be computed from the following relation:

$$\varepsilon(t) = \frac{\sqrt{\delta^2 + (\lambda/2)^2}}{\delta} - 1. \tag{3}$$

An important aspect of the UNCD specimens was that each membrane bowed upward as processed, i.e., out of the wafer plane. This is believed to result from the difference in thermal expansion coefficients, between the film and Si wafer, such that cooling down from the deposition temperature, approximately 800 °C, resulted in the Si shrinking more than the UNCD film. The film curvature is indicative of a gradient of residual stresses across the film thickness. The out-of-plane profile was obtained through interferometric measurements (Espinosa et al., 2003b). From this profile the height above the plane of the wafer, Δ_c, was determined. Also, the profile was used to measure the actual length of the curved membrane, which is used to determine the downward deflection, Δ_s, corresponding to the beginning of uniform specimen straining, see Fig. 3.

Next, we focus our attention on the two theoretically well-known limit cases of structures without defects, and structures with perfectly sharp cracks. They represents the limit case of micro-fabricated

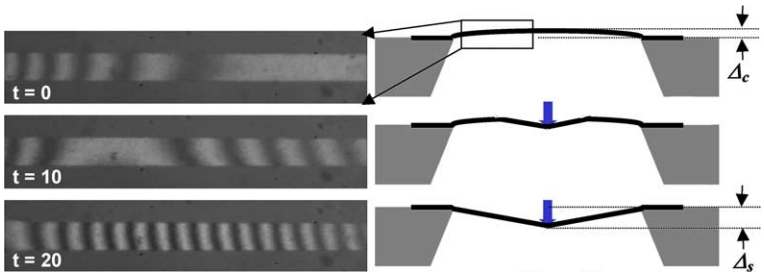

Fig. 3. Optical interferometric images of the UNCD specimen gauged region at 3 different time intervals with corresponding side-view schematic showing the profile of the membrane. Δ_c is the vertical displacement at the middle of the span and Δ_s is the deflection at which uniform straining of the membrane begins.

structures with defect length tending to zero (only pre-existing defects exist) and of micro-fabricated structures with blunt notch radius or corner angle tending to zero (sharp crack). The most general cases will be treated in subsequent sections.

3. Strength for MEMS structures without (micro-fabricated) defects

The stress–strain behavior obtained in a typical test considering a MEMS structure without micro-fabricated defects is shown in Fig. 4. The slope of the plot represents the elastic modulus, which was found to be 956 GPa. Modulus varied from 940 to 970 GPa for all the specimens tested (Espinosa et al., 2003b). Failure stress varied in a statistical manner. The fracture stress was in the range of 2.92–5.03 GPa (Espinosa et al., 2003c).

UNCD is a brittle material displaying a perfectly linear stress–strain response from zero strain to fracture, as we can see from Fig. 4. Lack of ductility or yielding leads to large data scatter in strength. The fracture strength of UNCD is determined by a combination of material microstructure and a variable defect size. As the fracture toughness is not variable, the variation must come from a variation in the size of the most critical defect. This is the reason why it is not possible to define the strength of UNCD as a constant material property but rather in terms of statistical parameters.

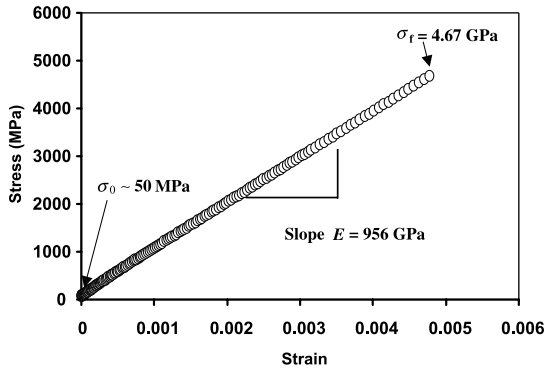

Fig. 4. Stress–strain curve representative of the behavior exhibited by a typical UNCD sample.

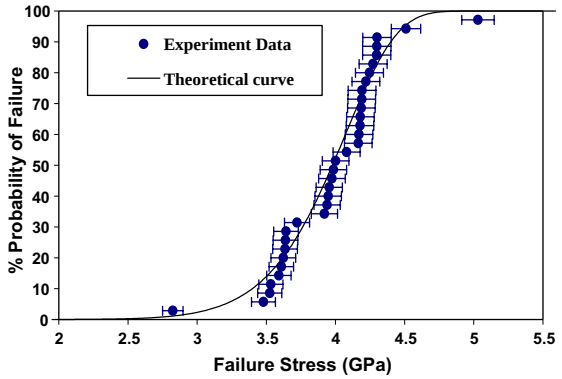

Fig. 5. Weibull plots for UNCD samples (Espinosa et al., 2003c).

It is known that the strength distribution of brittle materials does not follow a Gaussian distribution. Failure is described by the widely used Weibull cumulative function (Lawn, 1993; Sullivan and Lauzon, 1986; Nemeth et al., 2001). Weibull statistics allows examination of strength values in the sense of failure probability at a certain stress level. The Weibull distribution is defined as

$$P_{\mathrm{f}}(V) = 1 - \exp\left(-\frac{V}{V_0}\left(\frac{\sigma_{\mathrm{f}} - \sigma_{\mathrm{t}}}{\sigma_{\mathrm{n}}}\right)^m\right), \tag{4}$$

where σ_{f} is the failure stress, σ_{n} is the stress scaling parameter, in other words, it is the nominal stress that would result in 63%, $(1-e^{-1})\cdot 100\%$, of the specimens to fail, m is the Weibull modulus, which can be identified from a log–log plot of the probability of failure, σ_{t} is a threshold stress (in our case set to zero), and V_0 is the reference volume on which the Weibull parameters are identified. Here V/V_0 is assumed to be unity since the volume of the specimens was constant. For the validity of this formula in the context of MEMS materials see Peng et al. (2004). The Weibull plot is based on data obtained on a representative population of samples and, where possible, tested in a manner similar to those MEMS structures would experience during their lives. Thirty-four UNCD membranes were tested under the same environment using the proposed technique, with a higher than 97% success rate of failure.

The results of the fracture strength measurements are shown in Fig. 5 (Espinosa et al., 2003c). From plots of probability of failure and strength, the scaling parameter σ_{n} was identified as 4.18 GPa. The experimental data fit the Weibull distribution fairly well.

4. Strength of MEMS structures with sharp cracks

The fracture toughness, K_{IC}, can be determined using the membrane deflection technique by testing specimens possessing sharp cracks (Espinosa and Peng, 2004). The corresponding strength can be predicted for other geometries according to fracture mechanics. Sharp cracks were achieved by placing a Vickers indenter (with a 200 g load) near the specimen prior to its releasing. Although the indent was placed on the silicon substrate (see Fig. 6a) the radial crack initiated at one of the corners propagated into the UNCD specimen. The length of the crack was measured using high resolution scanning electron microscope (SEM), see Fig. 6b. In this configuration (edge crack), fracture toughness can be computed from the following equations (see Murakami, 1987):

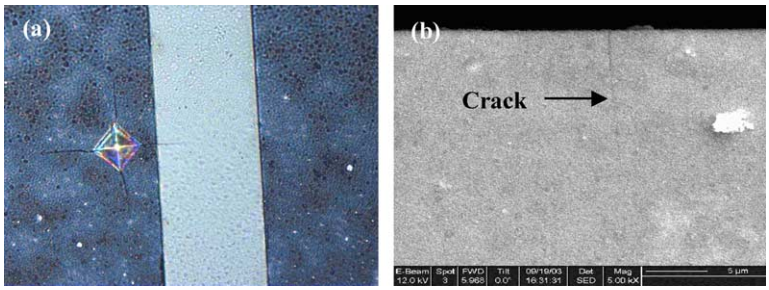

Fig. 6. (a) Optical image showing a sharp crack induced from an indent on the silicon substrate before the specimen was released, (b) SEM micrograph of the crack after the specimen was released. Crack length was measure from SEM images.

$$K_{\mathrm{IC}} = \sigma_{\mathrm{f}}\sqrt{\pi a} f\left(\frac{a}{W}\right), \tag{5}$$

$$f\left(\frac{a}{W}\right) = 1.12 - 0.23\left(\frac{a}{W}\right) + 10.55\left(\frac{a}{W}\right)^2 - 21.72\left(\frac{a}{W}\right)^3 + 30.41\left(\frac{a}{W}\right)^4, \tag{6}$$

where σ_{f} is the failure stress, a is the length of the crack and W is the width of the gauge region and $a/W \leqslant 0.6$.

Five specimens with sharp cracks were tested under the same condition except that the crack length, a, varied from 2.1 to 8.2 μm. The ratio of the crack length and specimen width, a/W, has a value in the range of 0.11–0.45. The fracture toughness of the UNCD membranes was computed using Eq. (5) and an average value of $K_{\mathrm{IC}} = 4.5 \pm 0.25$ MPa m$^{1/2}$ was obtained (Table 1). It is clear that K_{IC} is independent of crack length. This confirms that only the region of the material immediately in front of the pre-crack affects the material toughness.

5. Crack propagation criterion

We start by assuming the discrete crack propagation criterion suggested by Novozhilov (1969). Accordingly, a crack will propagate not when the stress reaches a critical value but when its integral along a finite length d_0 reaches a certain threshold. Consequently, the Novozhilov's brittle fracture criterion should be written in the following integral form:

$$\int_{d_0} \sigma_y(x)\,\mathrm{d}x \geqslant \sigma_{\mathrm{u}}\,\mathrm{d}_0, \tag{7}$$

where σ_{u} is a strength characteristic value for the material without defects (the ideal strength of the material at the characteristic size of d_0); $\sigma_y(x)$ represents the stress-field ahead of a defect with generic shape. This

Table 1
Fracture toughness measurement of MEMS structures

a (μm)	W (μm)	$\sigma_{\mathrm{f}}^{(\mathrm{exp})}$ (GPa)	K_{IC} (MPa m$^{1/2}$), Eq. (5)
2.1	18.1	1.35	4.1
3.9	18.2	0.95	4.4
5.8	18.0	0.80	4.8
6.6	18.2	0.71	4.5
8.2	18.1	0.75	4.4

criterion has been recently applied by Carpinteri and Pugno (2000, 2003) to predict the strength in structures containing re-entrant corners.

6. Strength of MEMS structures with blunt notches

For a blunt crack tip the asymptotic stress field is (Creager and Paris, 1967):

$$\sigma_y(x) = \frac{K_I}{\sqrt{2\pi x}}\left(1 + \frac{\rho}{2x}\right), \tag{8}$$

where the origin of the reference system is in the middle between the tip and the center of the circular blunt notch, so that $x > \rho/2$, where ρ is the root notch radius.

Drory et al. (1995) propose, comparing Eq. (8) and the case of a sharp crack ($\rho \to 0$), to obtain an equivalent stress-intensity factor for blunt notches, namely,

$$K'_{IC} = \left(1 + \frac{\rho}{2x}\right)K_{IC} \tag{9}$$

in which the variable x, as suggested by the same authors, is not well defined. They propose as a limit the "reasonable assumption" of $\rho/2x \to 1$. According to this limit case, they propose to estimate the real stress-intensity factor of the material K_{IC} simply dividing by a factor of 2 the measured stress-intensity factor K'_{IC} obtained from experiments on structures with blunt notches. On the other hand, focusing on the strength prediction, this assumption implies that crack blunting increases the component strength by a factor of 2.

On the other hand, by substituting the stress field (8) in Novozhilov's criterion, Eq. (7), we obtain the following condition for brittle crack propagation, as

$$\int_{\rho/2}^{\rho/2+d_0} \sigma_y(x, K_I = K'_{IC}, \rho)\,dx = \sqrt{\frac{2d_0}{\pi}}\frac{K'_{IC}}{\sqrt{1+\frac{\rho}{2d_0}}} = \sigma_u d_0. \tag{10}$$

For a sharp crack $\rho/2d_0 \to 0$ Eq. (10) becomes

$$\int_0^{d_0} \sigma_y(x, K_I = K_{IC}, \rho = 0)\,dx = \sqrt{\frac{2d_0}{\pi}}K_{IC} = \sigma_u d_0. \tag{11}$$

By comparing Eqs. (10) and (11), the asymptotic correction for $\rho/2d_0 \to 0$ on the stress-intensity factor due to the presence of blunting is obtained, i.e.,

$$K'_{IC} = \sqrt{1 + \frac{\rho}{2d_0}}K_{IC}, \tag{12}$$

so that the uncertainty in the value of x, as it is the case in Eq. (8), disappears.

The finite length d_0 is a material property and can be obtained (Carpinteri and Pugno, 2000, 2003) from Eq. (11):

$$d_0 = \frac{2}{\pi}\frac{K_{IC}^2}{\sigma_u^2}. \tag{13}$$

The ideal strength σ_u of the material, at the characteristic length of d_0, can be estimated from atomistic numerical simulations. On the other hand, d_0 can be obtained by matching two different experimental results performed on notches with different root radii ρ, as suggested by Eq. (12). Accordingly, for the tested UNCD we estimate d_0 by employing K'_{IC} (blunt notch with $\rho \approx 100$ nm of about 6.9 MPa m$^{1/2}$) and K_{IC} (sharp cracks), of about 4.5 MPa m$^{1/2}$, see Section 4. We have considered the smallest value of ρ because

the analysis is based on asymptotic behavior. The corresponding d_0 is estimated for the tested UNCD as $d_0^{\mathrm{UNCD}} \approx 37$ nm. Furthermore, from Eq. (13) we can estimate the *ideal strength* of the material at the characteristic size of d_0 as $\sigma_{\mathrm{u}}^{\mathrm{UNCD}} \approx 18.6$ GPa, which is consistent with the UNCD strength identified by Espinosa et al. (2003b,c) based on Weibull theory.

Instead of Eq. (5), according to our analysis, the blunt notch equivalent stress intensity factor is given by

$$K'_{\mathrm{IC}} = \sigma'_{\mathrm{f}}\sqrt{\pi a} f\left(\frac{a}{W}\right), \tag{14}$$

where σ'_{f} is the predicted strength in the case of blunting.

It is important to note that this analysis is asymptotic as a consequence of the considered asymptotic stress-field of Eq. (8). Accordingly for $\rho/2d_0 \to \infty$ it loses its validity, predicting $K'_{\mathrm{IC}} \to \infty$ and $\sigma'_{\mathrm{f}} \to \infty$. Practically, the collapse will arise in the ligament zone when the non asymptotic stress field will reach the ultimate strength of the material, i.e., $\sigma'_{\mathrm{f}}A = \sigma^*_{\mathrm{f}}A_{\mathrm{lig}}$, where σ^*_{f} (equal to σ_{n} defined in Section 3) is the failure stress for a membrane without additional defects (different from σ_{u} as a consequence of the pre-existing defects); A is the cross-section area of the membrane and A_{lig} is the cross-section of the ligament. Hence, substituting $\sigma'_{\mathrm{f}} = \sigma^*_{\mathrm{f}}A_{\mathrm{lig}}/A$ in the ratio between Eqs. (14) and (5) yields:

$$K'_{\mathrm{IC}} = K_{\mathrm{IC}}\frac{\sigma^*_{\mathrm{f}}A_{\mathrm{lig}}}{\sigma_{\mathrm{f}}A}. \tag{15}$$

As a consequence, the radius of curvature in Eq. (12) must be formally lower than

$$\frac{\rho^*}{2d_0} = \left(\frac{\sigma^*_{\mathrm{f}}A_{\mathrm{lig}}}{\sigma_{\mathrm{f}}A}\right)^2 - 1. \tag{16}$$

Note that ρ^* is a function of crack depth and specimen width. It also takes into account boundary effects. Hence, the resulting fracture toughness correction, as a function of notch radius ρ, is shown in Fig. 7.

Considering this limit case, the ratio $K'_{\mathrm{IC}}/K_{\mathrm{IC}}$ could became larger than 2, the limit case assumed by Drory et al. (1995), as we have experimentally observed (see Section 8). The other limit case of Eq. (12) is obviously $K'_{\mathrm{IC}} = K_{\mathrm{IC}}$.

Accordingly, the prediction for the strength in the case of blunt notches is the smaller value between the following:

$$\sigma'_{\mathrm{f}} = \sqrt{1 + \frac{\rho}{2d_0}}\sigma_{\mathrm{f}}, \quad \left(\frac{\rho}{\rho^*} \ll 1\right), \tag{17}$$

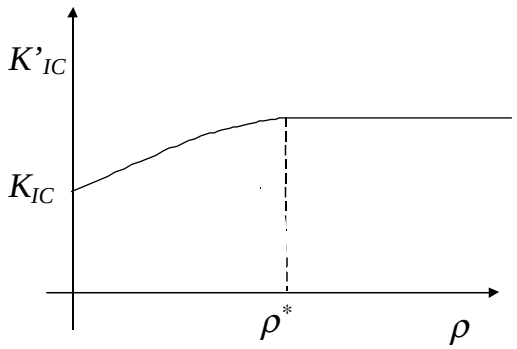

Fig. 7. Stress-intensity factor as a function of notch radius.

$$\sigma'_{\mathrm{f}} = \sigma^*_{\mathrm{f}} \frac{A_{\mathrm{lig}}}{A}, \quad \left(\frac{\rho}{\rho^*} \gg 1\right). \tag{18}$$

Eqs. (12) and (15) represent the corresponding corrections for the stress-intensity factor. The limit case of a sharp crack can be obtained for $\rho = 0$.

7. Strength of MEMS structures with re-entrant corners

A similar analysis can be performed for re-entrant corners (Carpinteri and Pugno, 2000, 2003). Williams (1952), proved that, when both the notch surfaces are free, the symmetrical stress field at the notch tip of a corner angle γ is

$$\sigma_y(x) = \frac{K^*_{\mathrm{I}}(\gamma)}{(2\pi x)^{\alpha(\gamma)}}, \tag{19}$$

where $K^*_{\mathrm{I}}(\gamma)$ is a generalized stress-intensity factor (note that its physical dimension changes with α, from a fracture toughness to a stress) as well as the power α of the stress singularity is provided by the eigen-equation:

$$(1-\alpha)\sin(2\pi-\gamma) = \sin[(1-\alpha)(2\pi-\gamma)] \tag{20}$$

and ranges between 1/2 (when $\gamma = 0$) and zero (when $\gamma = \pi$).

Substituting the stress field around the vertex of the corner (19) into Eq. (7), the condition for brittle crack propagation is obtained. Note that for the limit case of $\gamma = 0$ we obtain the same relation of Eq. (13) for the fracture quantum.

The problem here is more complex than the previous case of blunt tips, as a consequence of the changing in the physical dimensions of $K^*_{\mathrm{IC}}(\gamma)$. In spite of this, the result is very simple and considers automatically the non-asymptotical effects as shown by Carpinteri and Pugno (2000, 2003). The result can be summarized as follows:

$$\sigma''_{\mathrm{f}} = \sigma_{\mathrm{f}}^{2\alpha(\gamma)} \left(\sigma^*_{\mathrm{f}} \frac{A_{\mathrm{lig}}}{A}\right)^{1-2\alpha(\gamma)} \tag{21}$$

from which the strength σ''_{f} for (MEMS) structures with re-entrant corners can be predicted. In Eq. (21), σ_{f} and σ^*_{f} are the strength corresponding to the two well-defined limit cases (i) that of an ideal crack of the same length ($\gamma = 0$), (ii) and that of a simple cross-sectional reduction. Eq. (21) has been experimentally validated at the macro-scale by Carpinteri and Pugno (2000, 2003), starting from the experimental analysis performed by Carpinteri (1987).

According to Eqs. (5) and (14), in which $'$ is replaced by $''$, the correction for the stress-intensity factor is

$$K''_{\mathrm{IC}} = K_{\mathrm{IC}} \left(\frac{\sigma^*_{\mathrm{f}} A_{\mathrm{lig}}}{\sigma_{\mathrm{f}} A}\right)^{1-2\alpha(\gamma)}. \tag{22}$$

Eq. (22) predicts the same limit cases discussed in the previous section. The limit case of a sharp crack can be obtained for $\alpha = 1/2$.

8. Experimental assessment

A strength comparison between experimental results and theoretical predictions, based on Eqs. (17) and (18), for blunt notches, and on Eq. (21), for re-entrant corners, is given in Tables 2–4. The results are also

Table 2
Strength of MEMS structures as a function of the crack length ($\rho \approx 100$ nm)

a (μm)	W (μm)	$\sigma_f^{(exp)}$ (GPa) Experimental	σ'_f (GPa) Theory with notch correction Eq. (17)	σ_f (GPa) Theory without notch correction Eq. (5)
1.0	16.2	3.23	3.16	2.01
1.7	16.3	2.69	2.57	1.63
1.7	16.5	2.46	2.52	1.63
2.0	17.1	2.27	2.38	1.53
2.1	16.5	2.41	2.30	1.48
2.2	16.2	2.28	2.28	1.46
2.3	16.4	2.19	2.24	1.43
2.4	16.7	2.14	2.19	1.39
2.7	16.8	2.08	2.03	1.32
3.5	16.3	1.78	1.82	1.18
3.5	16.2	1.88	1.84	1.17
3.7	16.9	1.68	1.76	1.13
4.0	16.5	1.67	1.71	1.09
4.1	16.4	1.73	1.65	1.06
4.9	16.7	1.53	1.50	0.95

Table 3
Strength of MEMS structures as a function of the notch radius

ρ (nm)	a (μm)	W (μm)	$\sigma_f^{(exp)}$ (GPa) Experimental	σ'_f (GPa) Theory with Notch correction Eq. (17)	σ'_f (GPa) Theory with notch correction Eq. (18)	σ_f (GPa) Theory without notch correction Eq. (5)
100	2.4	16.2	2.04	1.94	(2.98)	1.25
140	2.2	16.1	2.25	2.29	(3.02)	1.32
170	2.1	16.1	2.50	2.28	(3.04)	1.23
220	1.4	16.3	3.52	(3.54)	3.20	1.74
230	1.2	16.2	3.55	(3.93)	3.24	1.90
490	2.2	16.2	2.85	(3.73)	3.02	1.32

Table 4
Strength of MEMS structures as a function of the re-entrant corner angle

γ (degree)	a (μm)	W (μm)	$\sigma_f^{(exp)}$ (GPa) Experimental	σ''_f (GPa) Theory on re-entrant corners Eq. (21)	σ_f (GPa) Theory on sharp-cracks Eq. (5)
16	8.0	18.2	0.39	0.36	0.38
79	5.4	17.6	0.73	0.70	0.60
92	10.2	18.1	0.25	0.21	0.26
101	3.0	17.5	1.45	1.35	1.06
120	10.1	18.3	0.41	0.43	0.23

compared to the trivial assumption of perfectly sharp cracks. In these tables, the influences of the crack length a, of the blunt notch radius ρ, and of the angle γ of the re-entrant corner are respectively analyzed. Several optical images of the micro-fabricated defects are reported in Table 5. In Table 3, the theoretical strength prediction is the smallest (not within brackets) between the two values as given by Eqs. (17) and (18). Note that the experimental cases for which we have found $\sigma'_f > 2\sigma_f$ indicate a departure from the correction proposed by Drory et al. (1995). Even if a clear scattering emerges from the experimental results, due to the statistics of pre-existing defect distribution (e.g., according to Weibull), as well as to the irregular geometry of the micro-fabricated defects, the analysis clearly shows that the corrections here derived cannot be neglected for an optimal MEMS structural design.

Table 5
SEM images of several micro-fabricated defects

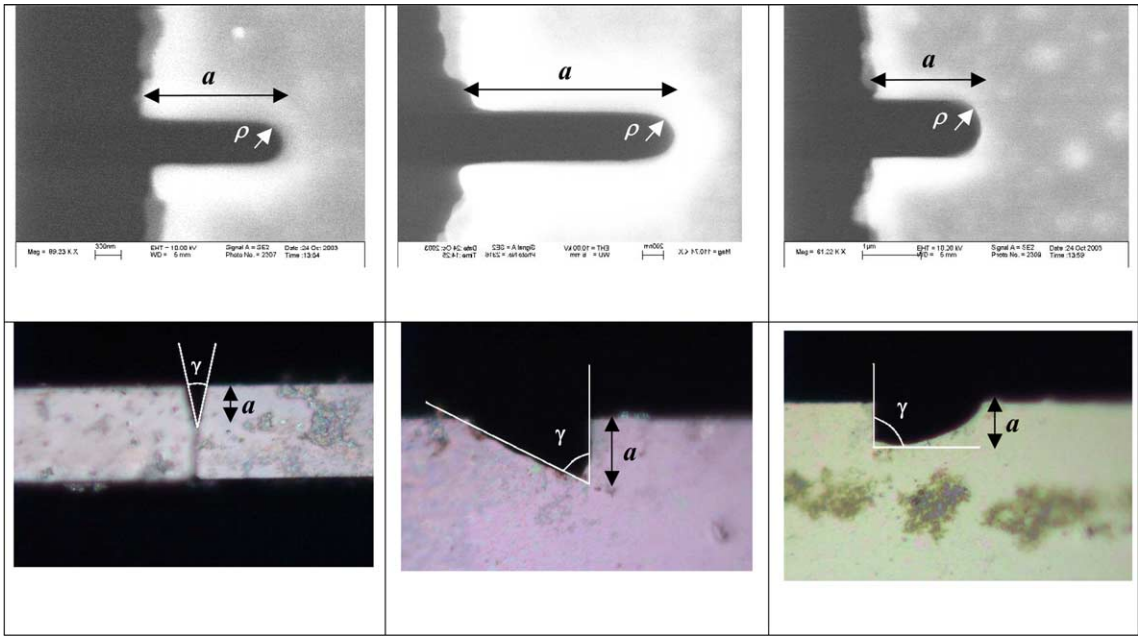

Table 6
Estimated mechanical parameters for the tested UNCD

UNCD: grain size (nm)	~5
d_0 (nm)	37
σ_f^* (GPa)	4.2
$\sigma_u(d_0)$ (GPa)	18.6
a_{eq} (μm)	0.3
E (GPa)	950
K_{IC} (MPa m$^{1/2}$)	4.5
G_{IC} (N/m)	20

By means of Eq. (5), the equivalent length of pre-existing (crack-like) defects in the UNCD material can be estimated. For $\sigma_f^* = 4.2$ GPa, stress corresponding to 67% probability of failure, a defect length $a_{eq} \approx 0.3$ μm is obtained. The fracture energy of the UNCD can be simply estimated as $G_{IC} = K_{IC}^2/E$, and it appears close to 20 N/m. In Table 6 the estimated set of mechanical properties for the tested UNCD are also reported.

9. Conclusions

We have proposed a novel experimental–theoretical method to investigate the strength and fracture of MEMS structures having complex defect geometries. We illustrated the applicability of the method by testing UNCD; although the method is general and applicable to many other materials. The main material

properties have also been estimated, showing that the proposed corrections for the stress-intensity factor cannot be neglected even for very small notch radius. In particular, a good agreement between theoretical prediction and experimental measurements of strength was obtained when varying crack length, notch radius and re-entrant corner angles were examined. This seems to suggest that the proposed analysis can be applied with confidence in the optimal structural design of MEMS.

Acknowledgments

This work was sponsored by the National Science Foundation under GOALI Award no. CMS-0120866/001. Work was also supported in part by the Nanoscale Science and Engineering Initiative of the National Science Foundation under NSF Award Number EEC-0118025 and by DOE Office of Science under contract no. N00014-97-1-0550. We thank Argonne National Laboratory for their support during the material processing. The authors would like to acknowledge N. Moldovan for assistance in the micro-fabrication of the specimens and many insightful suggestions.

References

Ballarini, R., Mullen, R.L., Yin, Y., Kahn, H., Stemmer, S., Heuer, A.H., 1997. The fracture toughness of polysilicon microdevices: a first report. J. Mater. Res. 12, 915–922.

Carpinteri, A., 1987. Stress-singularity and generalized fracture toughness at the vertex of re-entrant corners. Eng. Fract. Mech. 26, 143–155.

Carpinteri, A., Pugno, N., 2003. Fracture and collapse load for structural elements with re-entrant corners. Eng. Frac. Mech., in press.

Carpinteri, A., Pugno, N., Bari, 2000. Structural elements with re-entrant corners. In: Proc. of the XV National Congress Italian Group of Fracture (IGF), Italy, May 3–5, 2000, pp. 391–398.

Chasiotis, I., Knauss, W.G., 2000. Microtensile tests with the aid of probe microscopy for the study of MEMS materials. SPIE 4175, 92–99.

Chasiotis, I., Knauss, W.G., 2001. The influence of fabrication governed surface conditions on the mechanical strength of thin film materials. Mater. Res. Soc. Symp. Proc. 657, 221–226.

Chasiotis, I., Knauss, W.G., 2002. Size effects determined from tensile tests of perforated MEMS scale specimens. Mater. Res. Soc. Symp. Proc. 687, 241–246.

Creager, M., Paris, P.C., 1967. Elastic field equations for blunt cracks with reference to stress corrosion cracking. Int. J. Fract. Mech. 3, 247–252.

Drory, M., Dauskardt, R.H., Kant, A., Ritchie, R.O., 1995. Fracture of synthetic diamond. J. Appl. Phys. 78, 3083–3088.

Espinosa, H.D., Peng, B., 2004. A new methodology to investigate fracture toughness of freestanding MEMS and advanced materials in thin film form. J. MEMS 13 (4), in press.

Espinosa, H.D., Prorok, B.C., Fischer, M., 2003a. Methodology for determining mechanical properties of freestanding thin films and MEMS materials. J. Mech. Phys. Sol. 51, 47–67.

Espinosa, H.D., Prorok, B.C., Peng, B., Kim, K.-H., Moldovan, N., Auciello, O., Carlisle, J.A., Gruen, D.M., Mancini, D.C., 2003b. Mechanical properties of ultrananocrystalline diamond thin films relevant to MEMS devices. Exp. Mech. 43 (3), 256–268.

Espinosa, H.D., Peng, B., Prorok, B.C., Moldovan, N., Auciello, O., Carlisle, J.A., Gruen, D.M., Mancini, D.C., 2003c. Fracture strength of ultrananocrystalline diamond thin films—identification of Weibull parameters. J. Appl. Phys. 94 (9), 6076–6084.

Gruen, D., 1999. Nanocrystalline diamond films. Annu. Rev. Mater. Sci. 29, 211–259.

Jackson, K.M., Edwards, R.L., Dirras, G.F., Sharpe Jr., W.N., 2002. Mechanical properties of thin film silicon carbide. J. MEMS 687, 631–636.

Kahn, H., Tayebi, N., Ballarini, R., Mullen, R.L., Heuer, A.H., 2000. Fracture toughness of polysilicon MEMS devices. J. Sen. Act. 82, 274–280.

Lawn, B.R., 1993. Fracture of Brittle Solids, second ed. Cambridge University Press.

Murakami, Y. (Ed.), 1987. Stress Intensity Factors Handbook. Pergamon, Oxford.

Nemeth, N.N., Jadaan, O., Palko, J.P., Mitchell, J., Zorman, C.A., 2001. Proc. of the MEMS: Mech. and Meas. Symp., pp. 46–58.

Novozhilov, V., 1969. On a necessary and sufficient criterion for brittle strength. Prik. Mat. Mek. 33, 212–222.

Peng, B., Espinosa, H.D., Moldovan, N., Xiao, X., Auciello, O., Carlisle, J.A., 2004. Fracture Size effect in ultrananocrystalline diamond—application of Weibull Theory. J. Appl. Phys., submitted for publication.

Sharpe Jr., W.N., Turner, K.T., Edwards, R.L., 1999. Tensile testing of polysilicon. J. Exp. Mech. 39, 161–169.
Sharpe Jr., W.N., Jackson, K.M., Hemker, K.J., Xie, Z., 2001. Effect of specimen size on Young's modulus and fracture strength of polysilicon. J. MEMS 10, 317–326.
Sullivan, J.D., Lauzon, P.H., 1986. Experimental probability estimator for Weibull plots. J. Mater. Sci. Lett. 5, 1245–1247.
Williams, M.L., 1952. Stress singularities resulting from various boundary conditions in angular corners of plates in extension. J. Appl. Mech. 19, 526–528.